Rare Metal Materials and Engineering
Volume 51, Issue 7, July 2022
Available online at www.rmme.ac.cn

Science Press

Cite this article as: Gao Jingru, He Donglei, Guo Jiale, et al. Mechanical Properties, Biodegradation Behavior, and Cytocompatibility of As-Cast Mg-Ga Alloys for Bone Implant Applications[J]. Rare Metal Materials and Engineering, 2022, 51(07): 2379-2386.

ARTICLE

Mechanical Properties, Biodegradation Behavior, and Cytocompatibility of As-Cast Mg-Ga Alloys for Bone Implant Applications

Gao Jingru[1,2], He Donglei[1,2], Guo Jiale[1], Xue Xianda[1], Bi Yanze[1,2], Li Yan[1,2,3,4], Zheng Yang[5], Yu Hongyan[6]

[1] School of Materials Science and Engineering, Beihang University, Beijing 100191, China; [2] Beijing Advanced Innovation Center for Biomedical Engineering, Beihang University, Beijing 100191, China; [3] Key Laboratory of Aerospace Advanced Materials and Performance, Ministry of Education, Beihang University, Beijing 100191, China; [4] Hangzhou Innovation Institute, Beihang University, Hangzhou 310023, China; [5] School of Mechanical Engineering, Tiangong University, Tianjin 300387, China; [6] Beijing Key Laboratory of Radiation Advanced Materials, Beijing Research Center for Radiation Application, Beijing 100015, China

Abstract: The microstructures, mechanical properties, biodegradation behavior, and cytocompatibility of the as-cast Mg-2Ga and Mg-5Ga alloys were investigated. The microstructure characteristics were studied by X-ray diffractometer (XRD) and scanning electron microscopy (SEM). The results show that the Mg_5Ga_2 precipitates with globular and strip-like shapes are formed along the grain boundaries in Mg matrix after Ga addition. The grains of Mg-Ga alloys are obviously refined by Ga addition. The tensile tests reveal that the mechanical properties of Mg-Ga alloys are enhanced by Ga addition via solution strengthening, grain boundary strengthening, and precipitation strengthening. The electrochemistry and immersion corrosion tests in simulated body fluid at 37 °C reveal that the improved corrosion behavior is attributed to the enhanced surface stability caused by Ga addition of low content. In addition, the indirect contact assay suggests that both Mg-2Ga and Mg-5Ga alloys exhibit favorable cytocompatibility with no cytotoxicity for the mouse fibroblast (L929) cells.

Key words: biodegradable metals; Mg-Ga alloys; mechanical properties; biodegradation behavior; cytocompatibility

In recent years, Mg and its alloys attract much attention as the orthopedic implants and cardiovascular stents due to their favorable biocompatibility, unique biodegradability, and comparable elastic modulus to that of the natural bone[1-5]. Traditionally, the common commercial Mg alloys, such as AZ (Mg-Al-Zn) alloys, have been explored for their biomedical applications. However, it is increasingly difficult to satisfy the developing biosafety and bioactivity requirements because of the latent toxicity of Al element.

Recently, a series of biomedical Mg alloys, including Mg-Zn, Mg-Ca, Mg-Sr, and Mg-Sn, have been developed via addition of alloying elements[6-12]. Zhang[9] and Liu[10] et al compared the degradation and cytocompatibility of Mg-Sr and Mg-Ca-Sr alloys via direct culture with bone marrow derived mesenchymal stem cells, and found that the Mg-1Sr, Mg-1Ca-0.5Sr, and Mg-1Ca-1Sr alloys are potential candidates for skeletal implant applications. Mohamed et al[12] investigated the degradation and biocompatibility of Mg-0.8Ca alloy and proved its feasibility as bone implants and fixation devices. Nevertheless, the new-type biomedical Mg alloys are still required for improvement in clinical applications.

The gallium (Ga) element exhibits the similar nature to Al element, which may also enhance the mechanical properties of Mg alloys via solid solution strengthening and aging strengthening[13,14]. Besides, Ga can ameliorate the corrosion behavior of Mg alloys through microstructure change.

Received date: July 16, 2021
Foundation item: National Natural Science Foundation of China (51971014); Tianjin Municipal Natural Science Foundation (19JCQNJC02800); Beijing Municipal Natural Science Foundation (2182021)
Corresponding author: Li Yan, Ph. D., Professor, School of Materials Science and Engineering, Beihang University, Beijing 100191, P. R. China, Tel: 0086-10-82315989, E-mail: liyan@buaa.edu.cn

Furthermore, Ga has been investigated as an anti-carcinogen with broad-spectrum antibacterial effect[15-17]. Some preliminary researches have been conducted on the Mg-Ga alloys[18-21]. Mohedano et al[18] studied the microstructures of four as-cast binary Mg-*x*Ga (*x*=1, 2, 3, 4) alloys and found that two types of intermetallics (Mg_5Ga_2 and impurities) exist in the alloys. Kubasek et al[19] compared the mechanical properties and cytotoxicity of biodegradable Mg-*M* (*M*=Sn, Ga, In) alloys of 1wt%~7wt% alloying elements. It is found that Ga is the most effective element to improve the strength and toughness of Mg matrix and has the lowest toxic effect on human osteosarcoma (U-2 OS) cells. In addition, Gao et al[22] enhanced the antibacterial properties of pure Mg via micro-alloying with 0.1wt% Ga element. The Mg-0.1Ga alloy exhibits efficient suppression effect on the growth of gram-positive and gram-negative pathogens. Therefore, the Mg-Ga alloys may be suitable orthopedic implants for tissue repairment and infection treatment. However, few comprehensive researches were conducted on the relationship between microstructure and service performance of Mg-Ga alloys in the orthopedic applications. Thus, the mechanical properties, biodegradation behavior, and cytocompatibility of the as-cast Mg-2Ga and Mg-5Ga alloys in association with microstructure characterization were investigated in this research.

1 Experiment

The as-cast Mg-2Ga and Mg-5Ga alloys were prepared with the high-purity Mg (>99.99%) and high-purity Ga (>99.99%) in an electric resistance furnace under the protection of CO_2 and SF_6 mixture. The alloy melts were firstly purged at 780 °C protected by RJ-2 flux (37.1wt% KCl+43.2wt% $MgCl_2$+6.8wt% $BaCl_2$+4.8wt% CaF_2+6.6wt% [NaCl+$CaCl_2$] +1.3wt% water-insoluble substance+0.2wt% moisture), then held at 760 °C for 15 min for homogenization, poured into a mild steel crucible preheated at 720 °C, and finally cooled to room temperature.

The phase components were identified by an X-ray diffractometer (XRD, Model D/Max 2500 PC, Rigaku, Japan) with the Cu Kα radiation at a scan rate of 5°/min in 2θ=10°~90°. The surface morphology and phase distribution were observed by a field emission scanning electron microscope (SEM, ZEISS-SUPRA55, Germany) in the secondary electron (SE) and backscattered electron (BSE) mode.

The mechanical properties were evaluated via tensile tests at room temperature using a testing machine (MTS/SANS CMT7504) at a strain rate of 0.28 s^{-1}. The tensile specimens were machined from the cast ingots into the dog-bone-shaped specimen with the dimension of 30 mm×5 mm×3 mm by electro-discharge machining technique.

The biodegradation behavior was determined by both electrochemical corrosion and immersion corrosion tests in the simulated body fluid (SBF) at 37 °C. The chemical composition and preparation procedure of SBF are obtained from Ref.[23]. The electrochemical corrosion tests were performed at an electrochemical workstation (CHI660e, CH Instruments Inc., Shanghai, China) with a standard three-electrode system. The specimens with an exposed area of 1 cm^2, the platinum sheet, and the saturated calomel electrode (SCE) were served as the working electrode, counter electrode, and reference electrode, respectively. The potentiodynamic polarization curves were measured at a scan rate of 10 mV/s after immersion in SBF for 1 h for stabilization at the surface/solution interface. For the immersion corrosion tests, each specimen (10 mm×10 mm×2 mm) was immersed into 50 mL SBF, according to ASTM-G31-72. After immersion for 0.5, 1, 3, 5, 7, 14, 21, and 28 d, the specimens were rinsed with distilled water and dried in air. The pH value of SBF was recorded by a PHB-4 pH meter (INESA Scientific Instrument Co., Ltd, Shanghai). The corrosion products were removed by 200 g/L chromic acid solution. After that, the mass loss of specimens was measured by electronic scale with the scale of 0.01 mg in accuracy.

The static contact angles (θ) of ultra-pure water and ethylene glycol on the specimen surface were determined at room temperature by the contact angle goniometer (OCA-15, Dataphysics, Germany) using the sessile drop method. For each measurement, the testing liquid of 5 μL was dropped onto the surface at a dripping rate of 2 μL/s. After the stabilization, the drop profile was captured by the digital camera and its contact angle was calculated by the SCA-20 software. Five different regions on the surfaces of three specimens from each group were selected to obtain the average value of contact angles. Because the contact angle is sensitive to the surface condition, the measurements were conducted twice after settlement at room temperature for 30 and 100 h.

The surface free energy (SFE) γ can be calculated by the Owens-Wendt formula[24], as follows:

$$1+\cos\theta=[2(\gamma_s^d)^{1/2}(\gamma_l^d)^{1/2}+2(\gamma_s^p)^{1/2}(\gamma_l^p)^{1/2}]/\gamma_l \quad (1)$$

$$\gamma=\gamma_s^d+\gamma_s^p \quad (2)$$

where the γ_s^d and γ_s^p represent the solid SFE of the dispersive and polar components, respectively; γ_l^d and γ_l^p are the liquid SFE of the dispersive and polar components, respectively; γ_l is the liquid SFE. The γ_l^d and γ_l^p values can be obtained from Ref.[25].

The in-vitro cytotoxicity was evaluated via indirect contact assay according to GB/T 16886.5-2017. The mouse fibroblast (L929) cells were cultured using the Dulbecco's modified Eagle's medium (DMEM, Gibco, Australia) supplemented with 10vol% fetal bovine serum (FBS, GIBCO, Australia) in the 5vol% CO_2 incubator at 37 °C. The ratio of specimen surface area to the extraction medium was set as 3 cm^2/mL. The extracts with gradient contents (12.5vol%, 25vol%, 50vol%, 100vol%) were prepared with DMEM containing 10vol% FBS at 37 °C for 24 h. The L929 cells were seeded at a density of 1×10^5 mL^{-1} and incubated in 96-well cell culture plates for 24 h to facilitate cell attachment. Then, the culture medium was replaced by 100 μL extract (experimental group), DMEM (blank control), high-density polyethylene (HDPE, negative control), and DMEM containing 10vol%

dimethylsulfoxide (DMSO, positive control), separately. After that, the cells were incubated in a humid atmosphere of 5vol% CO_2 at 37 °C for 24 h. The cell morphology of the experimental group was captured by an inverted microscopy (IM, Olympus IX71-F22FL/DIC). The 3-(4,5-dimethylthiazol-2-yl)-2,5-diphenyltetrazolium bromide (MTT) assay was conducted to measure the cell viability by calculating the relative growth ratio (RGR) based on Eq.(3), as follows:

$$RGR=(A_{570\ nm}-A_{630\ nm})/(A^0_{570\ nm}-A^0_{630\ nm})\times 100\% \quad (3)$$

where A indicates the absorbance of the experimental group, negative control, and positive control; A^0 denotes the absorbance of the blank control; the subscript indicates the detective depth.

2 Results and Discussion

2.1 Microstructure

Fig.1 shows XRD patterns of the as-cast Mg-2Ga and Mg-5Ga alloys. The Mg-2Ga alloy is mainly composed of α-Mg phase, indicating that the Ga atom is almost dissolved into the α-Mg matrix. A small amount of Mg_5Ga_2 secondary phase can be detected in the Mg-5Ga alloy, as inferred by the characteristic diffraction peaks at 2θ=23.38°, 36.62°, 39.98° (standard PDF 97-010-3794). The maximum solid solubility of Ga in Mg is 8.5wt% at 420 °C and it is reduced with decreasing the temperature. The supersaturated Ga may form Mg_5Ga_2 secondary phase from the α-Mg matrix. The lattice constants of Mg-Ga alloys with hexagonal close-packed crystal structure are calculated from their XRD patterns by the Jade 5.0 software. The Mg-2Ga alloy exhibits the small lattice constants of a=0.320 94 nm and c=0.521 12 nm, compared with those of Mg-5Ga alloy (a=0.321 28 nm, c=0.521 50 nm). The Ga has smaller atomic size (0.135 nm) than Mg (0.160 nm) does, which leads to the expansion of unit cell by forming interstitial solid solution with higher Ga addition. Moreover, the c/a ratio of Mg-2Ga alloy (1.6237) and Mg-5Ga alloy (1.6232) is smaller than that of pure Mg (1.6241), which is a sign for lower activation energy barrier of additional slip planes and better plastic deformation[26].

Fig.2 presents SEM-BSE images of the as-cast Mg-2Ga and Mg-5Ga alloys. It is reported that the grains of as-cast pure Mg exhibit coarse equiaxed grain structure with average grain size of 150~400 μm, which depends on the casting procedures[27,28]. The addition of Ga element greatly refines the metallographic structure of as-cast pure Mg. It can be seen in Fig.2a that the Mg-2Ga alloy is characterized by α-Mg matrix (dark contrast) with equiaxed grain structure and some Mg_5Ga_2 precipitates (white contrast) randomly distributed along the grain boundaries. The segregation of Ga element (grey contrast) can be observed at the grain boundaries. As for the Mg-5Ga alloy, it exhibits the similar microstructure to Mg-2Ga alloy, but its grain size is smaller. The amount of Mg_5Ga_2 precipitates is obviously increased with increasing the Ga content from 2wt% to 5wt%. It can be observed that the Mg_5Ga_2 precipitates have the typical globular and strip-like morphologies. The similar morphologies of Mg_5Ga_2 precipitates can also be observed in the Mg-xGa (x=1, 2, 3, 4) alloys[18]. In addition, no Mg_5Ga_2 phase can be detected in the XRD pattern of Mg-2Ga alloy, which may be attributed to its low content.

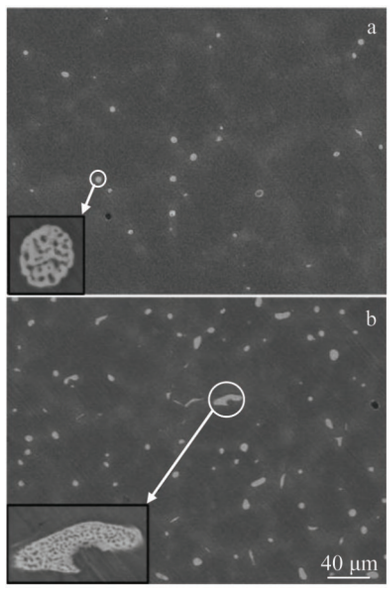

Fig.2 SEM-BSE images of as-cast Mg-2Ga (a) and Mg-5Ga (b) alloys

2.2 Mechanical properties

Fig. 3 shows the tensile stress-strain curves of the as-cast Mg-2Ga and Mg-5Ga alloys. The yield stress (YS), ultimate

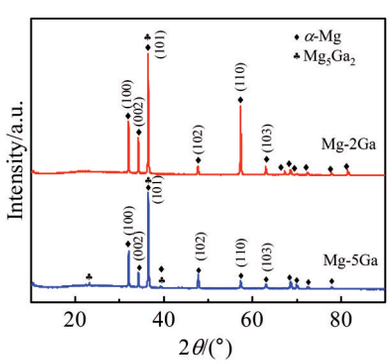

Fig.1 XRD patterns of as-cast Mg-2Ga and Mg-5Ga alloys

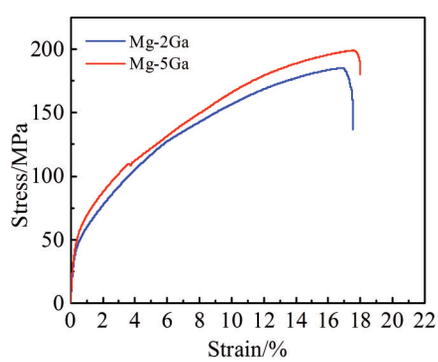

Fig.3 Tensile stress-strain curves of as-cast Mg-2Ga and Mg-5Ga alloys

tensile stress (UTS), and elongation (EL) of Mg-2Ga alloy is 57 MPa, 184 MPa, and 16%, respectively. The higher YS of 80 MPa, UTS of 198 MPa, and EL of 18% are achieved for the Mg-5Ga alloy. The strengthening effect of Ga element on pure Mg can be ascribed to the following aspects: (1) the increasing Ga content can refine the grain size and induce grain boundary strengthening according to the Hall-Petch relationship[29]; (2) more Mg_5Ga_2 precipitates are formed at the grain boundaries with higher Ga content, therefore effectively hindering the grain boundary movement during tensile deformation by precipitation strengthening[30]; (3) Ga addition leads to the lattice distortion as a result of the atomic diameter difference between Mg and Ga, which can enhance the α-Mg matrix via solid solution strengthening[29].

The comparisons of mechanical properties of biomedical pure and binary Mg alloys are summarized in Table 1. The mechanical properties of pure Mg alloy can hardly satisfy the clinical application requirements. Therefore, various biocompatible alloying elements (Zn, In, Sn) have been introduced to improve the mechanical properties of Mg alloys. For example, the Mg-Zn alloys containing 1wt%~7wt% Zn possess YS of 20~76 MPa, UTS of 102~217 MPa, and EL of 6%~18%. The Mg-2Ga and Mg-5Ga alloys in this research exhibit comparable strength (YS of 57~80 MPa, UTS of 184~198 MPa) and superior elongations (16%~18%). These excellent comprehensive mechanical properties of Mg-2Ga and Mg-5Ga alloys show their application potential as orthopedic implants[31].

Fig.4 shows the morphologies of fracture surfaces of the as-cast Mg-2Ga and Mg-5Ga alloys. The failure of Mg-2Ga alloy is dominated by cleavage fracture, as indicated by the step-like fracture morphology in Fig.4a. There also exist some tiny dimples on the fracture surface, suggesting that the fracture of Mg-2Ga alloy is accompanied by slight plastic deformation.

Table 1 Mechanical properties of biomedical pure Mg and binary Mg alloys

Alloy	YS/MPa	UTS/MPa	EL/%	Ref.
Pure Mg	20~30	85~120	4.8~13	[19,32,33]
Mg-1Zn	20~61	102~188	7~18	[32-34]
Mg-2Zn	65	180	14	[35]
Mg-4Zn	58	217	16	[34]
Mg-5Zn	76	195	8.5	[32]
Mg-7Zn	67	136	6	[32]
Mg-3In	25	100	5.3	[19]
Mg-5Sn	53	134	3.8	[19]
Mg-4Ga	66	188	7.2	[19]
Mg-2Ga	57	184	16	-
Mg-5Ga	80	198	18	-

As shown in Fig. 4b, the similar fracture morphology can be observed for the Mg-5Ga alloy with much more dimples, which implies better plastic deformation ability. As shown in Fig. 4c and 4d, lots of Ga enrichment sites are found at the dimples on the fractured surfaces of Mg-2Ga and Mg-5Ga alloys, indicating a positive relationship between the ductility and Ga content.

2.3 Biodegradation behavior

Fig. 5 displays the potentiodynamic polarization curves of the as-cast pure Mg, Mg-2Ga, and Mg-5Ga alloys in SBF at 37 °C. The anodic branch and cathodic branch represent the metal dissolution by oxidation and hydrogen evolution via water reduction, respectively[36]. The corresponding electrochemical parameters of corrosion potential (E_{corr}), corrosion current density (i_{corr}), anodic Tafel slope (β_a), and cathodic Tafel slope (β_c) are summarized in Table 2. Compared with the E_{corr} of −1884±20 mV and i_{corr} of 282±55 μA/cm^2 of pure Mg,

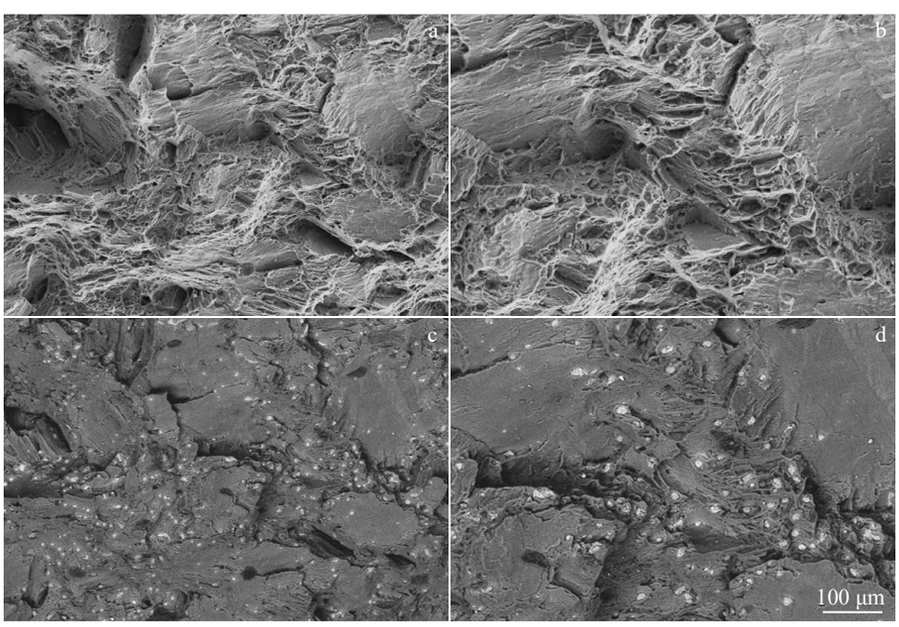

Fig.4 SEM morphologies in SE (a, b) and BSE (c, d) images of fracture surfaces in as-cast Mg-2Ga (a, c) and Mg-5Ga (b, d) alloys

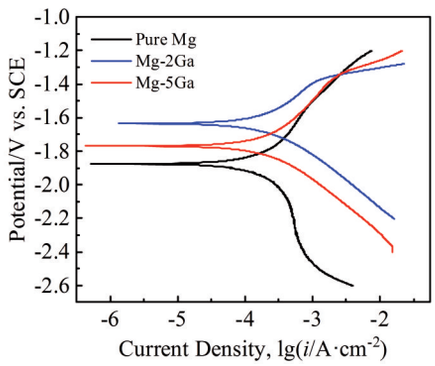

Fig.5 Potentiodynamic polarization curves of the as-cast pure Mg, Mg-2Ga and Mg-5Ga alloys in 37 °C SBF

Table 2 Electrochemical parameters of as-cast pure Mg, Mg-2Ga, and Mg-5Ga alloy samples fitted from potentiodynamic polarization curves

Sample	E_{corr}/mV	i_{corr}/μA·cm^{-2}	β_a	β_c
Pure Mg	−1884±20	282±55	4.6±0.3	4.4±0.2
Mg-2Ga	−1641±52	154±39	5.0±0.2	5.7±0.2
Mg-5Ga	−1773±14	170±48	4.9±0.2	5.7±0.3

the Mg-2Ga alloy presents a higher E_{corr} of −1641±52 mV and a lower i_{corr} of 154±39 μA/cm^2, indicating that better corrosion resistance is obtained with 2wt% Ga addition. However, the slightly inferior corrosion resistance is found for the Mg-5Ga alloy, which may be due to the accelerated galvanic corrosion induced by the excess Mg_5Ga_2 precipitates[18]. Furthermore, the Tafel slopes of Mg-2Ga and Mg-5Ga alloys are larger than those of pure Mg, demonstrating that the higher polarization resistance is obtained for the Mg-2Ga and Mg-5Ga alloys.

Fig.6 summarizes the pH value of SBF and mass loss ratio of the as-cast pure Mg, Mg-2Ga, and Mg-5Ga alloys during immersion tests in SBF at 37 °C. Fig.6a shows that the pH value increases linearly to 10.51, 9.97, and 9.85 for pure Mg (3 d), Mg-2Ga (5 d), and Mg-5Ga (5 d) alloys, respectively. Then the pH value remains relatively stable with increasing the immersion time. This change trend of pH value can be explained by the following facts[9,37]. In the initial stage of immersion, the magnesium hydroxide ($Mg(OH)_2$) is firstly formed via chemical reaction of $Mg+2H_2O=Mg(OH)_2+H_2$, and then it is transformed into the soluble $MgCl_2$, which releases extra OH^- and results in alkalization of SBF. After that, the pH value becomes steady as the OH^- content reaches the saturation state. Fig.6b presents that the mass loss ratios of pure Mg, Mg-2Ga, and Mg-5Ga alloys continuously increase during immersion for 28 d. Both Mg-2Ga and Mg-5Ga alloys have lower corrosion rate than pure Mg does during immersion for 7 d, which is consistent with the results of electrochemical corrosion tests (Fig.5 and Table 2). However, the significant increase in mass loss ratio is observed for the Mg-5Ga alloy with the immersion proceeding from 7 d to 28 d, which suggests that the corrosion resistance is reduced with

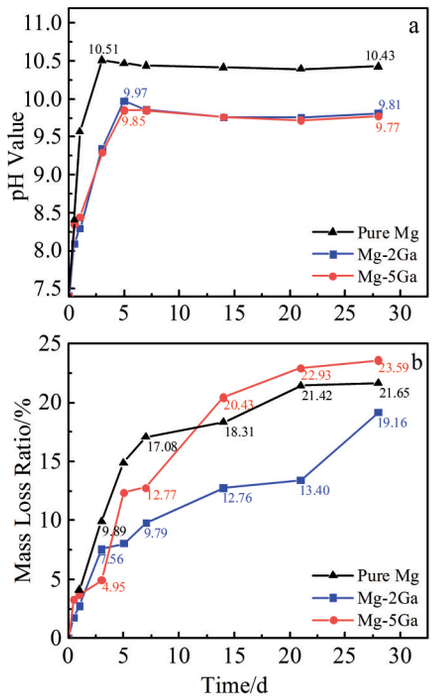

Fig.6 pH values of SBF (a) and mass loss ratios (b) of as-cast pure Mg, Mg-2Ga, and Mg-5Ga alloys during immersion in SBF at 37 °C

increasing Ga content. Two opposite effects of Ga element are found for the corrosion behavior of Mg-Ga alloys: (1) the solid solution Ga with higher standard potential (−0.55 V) enhances the surface stability of Mg-Ga alloys and increases the corrosion resistance of Mg alloys; (2) the supersaturated Ga element produces Mg_5Ga_2 precipitates at the grain boundaries of Mg-Ga alloys, which generates galvanic corrosion and increases the corrosion rate. Therefore, the corrosion behavior of Mg-Ga alloys can be improved by a small amount of Ga addition.

2.4 Biocompatibility

Fig.7 illustrates the contact angles of water and glycol on the surface of as-cast pure Mg, Mg-2Ga, and Mg-5Ga alloys. The contact angle indicates the wettability at the solid-liquid interface: the smaller the contact angle θ, the better the spreading ability of alloy. The water contact angle is related to the hydrophilia, whereas the glycol contact angle represents the hydrophobicity on the surface. It can be seen in Fig.7a that the water contact angle (65±3.5°) and glycol contact angle (70±3.8°) of pure Mg are larger than those of Mg-2Ga and Mg-5Ga alloys after settlement at room temperature for 30 h, suggesting that better wettability is obtained after Ga addition. With the settlement further proceeding to 100 h, as shown in Fig.7b, the water and glycol contact angles of pure Mg, Mg-2Ga, and Mg-5Ga alloys are basically the same. This change trend for contact angles with the settlement proceeding is due to the formation of oxidation on the alloy surface.

SFE (γ) of as-cast pure Mg, Mg-2Ga, and Mg-5Ga alloys is calculated and shown in Table 3. It is noted that γ is composed

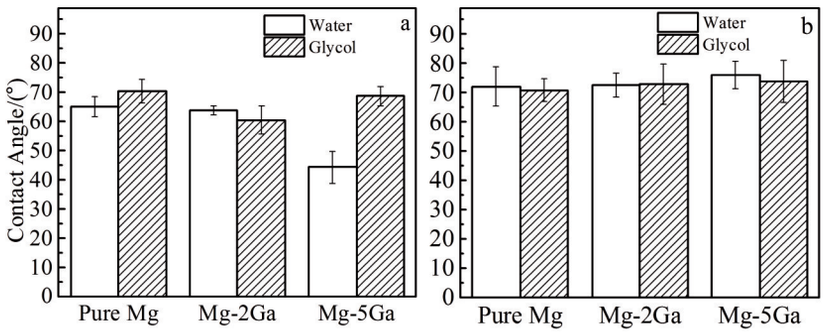

Fig.7 Contact angles of water and glycol on the surface of as-cast pure Mg, Mg-2Ga, and Mg-5Ga alloys for 30 h (a) and 100 h (b)

Table 3 SFEs of as-cast pure Mg, Mg-2Ga, and Mg-5Ga alloys after settlement for different durations (mJ/m^2)

SFE	Pure Mg		Mg-2Ga		Mg-5Ga	
	30 h	100 h	30 h	100 h	30 h	100 h
γ_s^p	9.905	4.192	4.035	4.990	34.065	3.322
γ_s^d	40.901	52.434	69.933	47.112	19.401	50.034
γ	50.806	56.625	73.968	52.102	53.465	53.356

of polar component (γ_s^p) and dispersive component (γ_s^d), where the γ_s^p represents the hydrophilia and the γ_s^d indicates the hydrophobicity[38]. The γ of Mg-2Ga alloy (73.968 mJ/m^2) and Mg-5Ga alloy (53.465 mJ/m^2) is larger than that of pure Mg (50.806 mJ/m^2) after settlement for 30 h. Then the γ of the three alloys is changed with increasing the settlement time to 100 h, and finally shows the similar values. The higher SFE of Mg-Ga alloys in the initial stage indicates the better wettability Mg-Ga alloys compared with that of pure Mg, which may be beneficial to the adhesion and spread of anchorage-dependent cells on the surface[39].

Fig. 8 shows the cell morphologies of L929 cells after culture in different extracts with various contents for 24 h. It can be seen from Fig. 8a that the L929 cells cultured by DMEM grow well into the typical spindle shape. Likewise, the L929 cells in the 100vol% and 12.5vol% Mg-Ga extracts are healthy and vibrant to spread evenly on the surface. Whereas in Fig. 8b and 8e, the growth and proliferation of L929 cells are hindered by pure Mg extracts, particularly the one of 100vol%, which may be caused by the relatively strong alkalinity due to the fast corrosion of pure Mg alloy.

RGR and cytotoxicity levels of L929 cells cultured by pure Mg, Mg-2Ga, and Mg-5Ga extracts with different contents are listed in Table 4. The cytotoxicity is rated as four levels: level 0 (RGR≥100%), level 1 (99%≥RGR≥80%), level 2 (79%≥RGR≥50%), and level 4 (50%≥RGR). The Mg-2Ga and Mg-5Ga alloys have obviously lower cytotoxicity level (level 0) than pure Mg (level 1 and level 4) does, which implies that the addition of Ga element is beneficial for the growth and

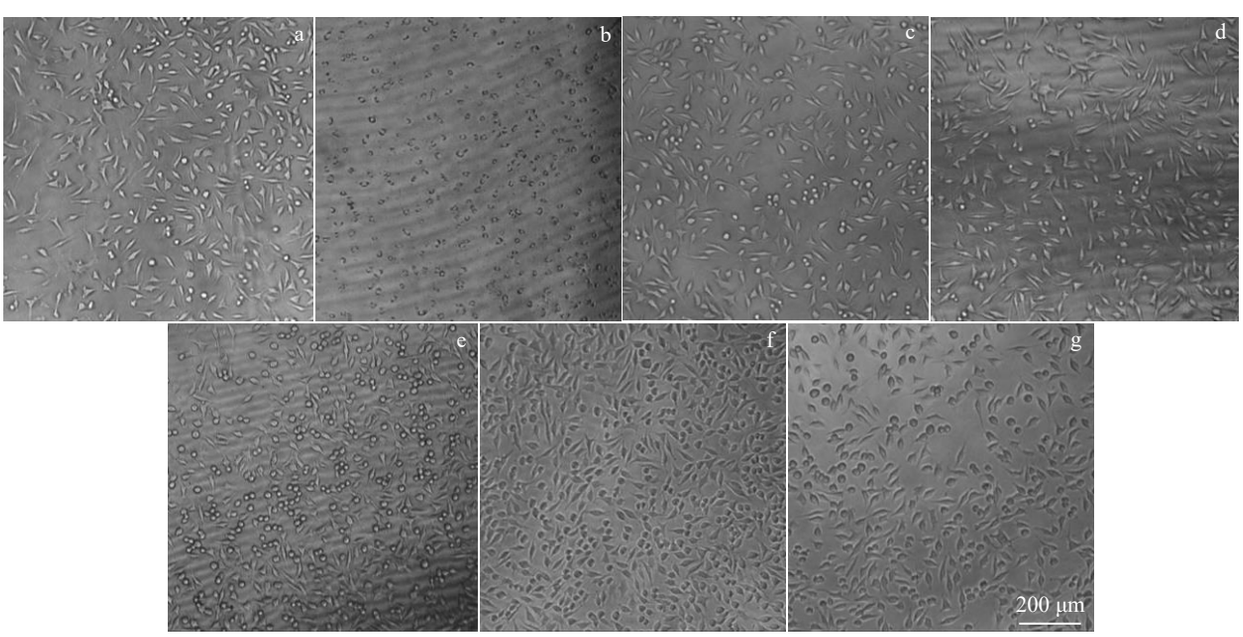

Fig.8 Morphologies of L929 cells cultured by DMEM (a), pure Mg (b, e), Mg-2Ga (c, f), and Mg-5Ga (d, g) extracts with contents of 100vol% (b~d) and 12.5vol% (e~g)

Table 4 RGRs and cytotoxicity levels of L929 cells cultured by pure Mg, Mg-2Ga, and Mg-5Ga extracts with different contents

Culture medium	Content/vol%	RGR/%	Cytotoxicity level
Blank control	-	100.00	-
Negative control	-	109.60	0
Positive control	-	23.22	4
Pure Mg	12.5	105.88	0
	25	98.41	1
	50	111.68	0
	100	4.71	4
Mg-2Ga	12.5	115.58	0
	25	114.53	0
	50	113.93	0
	100	119.54	0
Mg-5Ga	12.5	119.15	0
	25	114.39	0
	50	111.73	0
	100	106.79	0

proliferation of L929 cells. As reported in Ref. [33], the relative viability of L929 cells cultured by Mg-1Zn alloy extract is approximately 119% after culture for 2 d. However, the RGR of L929 cells cultured by 100vol% Mg-2Ga extract can reach 119.54% with much shorter culture time, indicating that the Mg-2Ga alloy has better cytocompatibility.

3 Conclusions

1) The Mg-2Ga and Mg-5Ga alloys are composed of α-Mg phase with equiaxed grain structure and Mg_5Ga_2 secondary phase distributed along the grain boundaries. The Mg_5Ga_2 precipitates exhibit globular and strip-like shapes and their amount is increased with increasing the Ga addition. The grain size of alloys is also reduced by Ga addition.

2) The mechanical properties of pure Mg alloy are greatly improved after Ga addition by the combined effects of solution strengthening, grain boundary strengthening, and precipitation strengthening. The highest yield strength, ultimate tensile strength, and elongation reach 80 MPa, 198 MPa, and 18% for the Mg-5Ga alloy.

3) The corrosion behavior of Mg-Ga alloy is improved by Ga addition. The addition of low content of 2wt% Ga enhances the corrosion resistance via improving the surface stability, whereas the large addition of 5wt% Ga increases the corrosion rate by forming excess galvanic corrosion.

4) The surface wettability is improved by Ga addition. Better cell adhesion and growth behavior can be obtained for the Mg-Ga alloys. Both Mg-2Ga and Mg-5Ga alloys exhibit favorable cytocompatibility for L929 cells without cytotoxicity.

References

1 Qiao Xueyan, Yu Kun, Chen Liangjian *et al*. *Rare Metal Materials and Engineering*[J], 2018, 47(3): 773

2 Song Mingshi, Zeng Rongchang, Ding Yunfei *et al*. *Journal of Materials Science & Technology*[J], 2019, 35(4): 535

3 Ali M, Hussein M A, Al-Aqeeli N. *Journal of Alloys and Compounds*[J], 2019, 792: 1162

4 Kiani F, Wen C E, Li Y C. *Acta Biomaterialia*[J], 2020, 103: 1

5 Zheng Y F, Gu X N, Witte F. *Materials Science and Engineering R*[J], 2014, 77: 1

6 Yang M, Liu D B, Zhang R F *et al*. *Rare Metal Materials and Engineering*[J], 2018, 47(1): 93

7 Jiang W S, Cipriano A F, Tian Q M *et al*. *Acta Biomaterialia*[J], 2018, 72: 407

8 Shi W, Zhao D P, Shang P *et al*. *Rare Metal Materials and Engineering*[J], 2018, 47(8): 2371

9 Zhang S Y, Zheng Y, Zhang L M *et al*. *Materials Science and Engineering C*[J], 2016, 68: 414

10 Liu J N, Bian D, Zheng Y F *et al*. *Acta Biomaterialia*[J], 2020, 102: 508

11 Li Y, Liu L N, Wan P *et al*. *Biomaterials*[J], 2016, 106: 250

12 Mohamed A, El-Aziz A M, Breitinger H G *et al*. *Journal of Magnesium and Alloys*[J], 2019, 7(2): 249

13 Cáceres C H, Rovera D M. *Journal of Light Metals*[J], 2001, 1(3): 151

14 Teng J W, Gong X J, Li Y P *et al*. *Materials Science and Engineering A*[J], 2018, 715: 137

15 Timerbaev A R. *Metallomics*[J], 2009, 1(3): 193

16 Thompson M G, Truong-Le V, Alamneh Y A *et al*. *Antimicrobial Agents and Chemotherapy*[J], 2015, 59: 6484

17 Antunes L, Imperi F, Minandri F *et al*. *Antimicrrobial Agents and Chemotherapy*[J], 2012, 56: 5961

18 Mohedano M, Blawert C, Yasakau K A *et al*. *Materials Characterization*[J], 2017, 128: 85

19 Kubasek J, Vojtech D, Lipov J *et al*. *Materials Science and Engineering C*[J], 2013, 33(4): 2421

20 Liu H B, Qi G H, Ma Y T *et al*. *Materials Science and Engineering A*[J], 2009, 526(1-2): 7

21 Huang W S, Chen J H, Yan H G *et al*. *Metals and Materials International*[J], 2020, 26: 747

22 Gao Z H, Song M S, Liu R L *et al*. *Materials Science and Engineering C*[J], 2019, 104: 109 926

23 Kokubo T, Takadama H. *Biomaterials*[J], 2006, 27(15): 2907

24 Zhao T T, Li Y, Zhao X Q *et al*. *Journal of Biomedical Materials Research*[J], 2012, 100(3): 646

25 Owens D K, Wendt R C. *Journal of Applied Polymer Science*[J], 1969, 13(8): 1741

26 Mendis C L, Bettles C J, Gibson M A *et al*. *Materials Science and Engineering A*[J], 2006, 435-436: 163

27 Li W T, Shen Y N, Shen J *et al*. *Nano Materials Science*[J],

2020, 2(1): 96
28 Ocal E B, Esen Z, Aydinol K *et al*. *Materials Chemistry and Physics*[J], 2020, 241: 122 350
29 Gui Y W, Cui Y J, Bian H K *et al*. *Journal of Alloys and Compounds*[J], 2020, 856: 158 201
30 Pan H C, Qin G W, Xu M *et al*. *Materials and Design*[J], 2015, 83: 736
31 Ding W J. *Regenerative Biomaterials*[J], 2016, 3(2): 79
32 Cai S H, Lei T, Li N F *et al*. *Materials Science and Engineering C*[J], 2012, 32(8): 2570
33 Gu X N, Zheng Y F, Cheng Y *et al*. *Biomaterials*[J], 2009, 30(4): 484
34 Zhang B P, Wang Y, Geng L. *Biomaterials: Physics and Chemistry*[M]. Shanghai: Intech, 2011: 183
35 Zareian Z, Emamy M, Malekan M *et al*. *Materials Science and Engineering A*[J], 2020, 774: 138 929
36 Zheng Y, Ma Y L, Zang L B *et al*. *Materials and Corrosion*[J], 2019, 70(12): 2292
37 Zhang S X, Li J N, Song Y *et al*. *Materials Science and Engineering C*[J], 2009, 29(6): 1907
38 Busscher H J. *Modern Approaches to Wettability*[M]. Berlin: Springer, 1992: 249
39 Ma J W, Zan R, Chen W Z *et al*. *Rare Metals*[J], 2019, 38(6): 543

骨植入用铸态Mg-Ga合金的力学性能、生物降解行为及细胞相容性

高静如[1,2]，何东磊[1,2]，郭佳乐[1]，薛贤达[1]，毕衍泽[1,2]，李　岩[1,2,3,4]，郑　洋[5]，于宏燕[6]

(1. 北京航空航天大学 材料科学与工程学院，北京 100191)

(2. 北京航空航天大学 北京生物医学工程高精尖创新中心，北京 100191)

(3. 北京航空航天大学 空天先进材料与服役教育部重点实验室，北京 100191)

(4. 北京航空航天大学 杭州创新研究院，浙江 杭州 310023)

(5. 天津工业大学 机械工程学院，天津 300387)

(6. 北京市射线应用研究中心 辐射新材料北京市重点实验室，北京 100015)

摘　要：研究了铸态Mg-2Ga和Mg-5Ga合金的力学性能、生物腐蚀行为、细胞相容性与其微观组织结构的变化关系。采用X射线衍射仪（XRD）和扫描电子显微镜（SEM）对材料的微观组织结构进行了分析。结果表明：添加Ga元素后，在镁基体的晶界上形成了球状和带状的Mg_5Ga_2析出相，Ga元素显著细化了镁基体的晶粒尺寸。力学拉伸试验结果表明，Ga元素可通过固溶强化、晶界强化、析出强化等作用提高Mg-Ga合金的力学性能。在37 ℃模拟体液中的电化学腐蚀和浸泡腐蚀试验结果表明，低Ga含量能够提高Mg-Ga合金的表面稳定性，从而改善其腐蚀行为。此外，间接接触细胞培养试验结果表明，Mg-2Ga与Mg-5Ga合金均对小鼠成纤维细胞（L929）表现出良好的细胞相容性，未对其产生明显的细胞毒性。

关键词：生物降解金属；镁稼合金；力学性能；生物降解行为；细胞相容性

作者简介：高静如，女，1996年，硕士，北京航空航天大学材料科学与工程学院，北京 100191，E-mail：jill_g@buaa.edu.cn